Amphiprotism-Coupled Near-Infrared Emission in Extended Pyrazinacenes Containing Seven Linearly Fused Pyrazine Units

Gary J Richards, Aël Cador, Shinji Yamada, Anna Middleton, Whitney A Webre, Jan Labuta, Paul A Karr, Katsuhiko Ariga, Francis d'Souza, Samia Kahlal, et al.

Amphiprotism-coupled NIR-Emission in Extended Pyrazinacenes containing Seven Linearly-fused Pyrazine Units

Gary J. Richards,*[,†,#] Aël Cador,[‡] Shinji Yamada,[†] Anna Middleton,[§] Whitney A. Webre,[§] Jan Labuta,[#] Paul A. Karr,[¶] Katsuhiko Ariga,[#,⊥] Francis D'Souza,[§] Samia Kahlal,[‡] Jean-François Halet,[‡] and Jonathan P. Hill*[,#]

[†]Department of Chemistry, Ochanomizu University, Otsuka 2-1-1, Bunkyo-ku, Tokyo 112-8610, Japan

[#]International Center for Materials Nanoarchitectonics, National Institute for Materials Science Namiki 1-1, Tsukuba, Ibaraki 305-0044, Japan

[‡]Univ Rennes, CNRS, Institut des Sciences Chimiques de Rennes (ISCR) – UMR 6226, 35000 Rennes, France

[§]Department of Chemistry, University of North Texas, 1155 Union Circle, 305070 Denton, Texas 76203, USA

[¶]Department of Physical Sciences and Mathematics, Wayne State College, 111 Main Street, Wayne, Nebraska, 68787, USA

[⊥]Graduate School of Frontier Sciences, The University of Tokyo, Kashiwa 277-0827, Japan

Supporting Information Placeholder

ABSTRACT: Peripherally substituted tetradecaazaheptacene (N_{14}Hp) compounds, exhibiting amphiprotism-coupled emission, have been synthesized. X-ray crystallography reveals a planar acene-like chromophore, and electronic absorption and emission occur in the near infrared biological transparency window (650 – 900 nm). The compounds exhibit long wave emission with photoluminescence quantum yields Φ_{PL} up to ~0.61 at 686 nm with monodeprotonated state Φ_{PL} ~0.58 at 712 nm. This unprecedented highly nitrogenous chromophore illustrates the stability and utility of the pyrazinacenes for different applications based on their photophysical properties and chemical structures.

Pyrazinacenes[1,2] contain multiple 1,4-pyrazine units linearly-fused through C-C bonds so that the nitrogen atoms are contained at the apical positions of the acene framework. Higher analogues tend to contain a single reduced dihydropyrazine because of the relative electron deficiency of these highly nitrogenous chromophore molecules.[1-3] On the other hand, chromophore-based bio-imaging techniques rely on the availability of dyes that are emissive in regions of the electromagnetic spectrum not obscured by absorptive processes of biomolecules or water.[4,5] Thus, dyes emitting in the near-infrared transparency window region of tissues from 650-900 nm are useful for imaging,[6] also allowing good tissue penetration without significant risk of damage caused by ultraviolet light. It is also advantageous if excitation and emission wavelengths of a particular chromophore lie within this region with the additional benefit that tissue autofluorescence is minimized. Several classes of dye meet these requirements including cyanines (e.g., ICG)[7], BODIPY[8] and porphyrins.[9] Despite the availability of these dyes, the development of new synthetically flexible dyes as NIR-emitting chromophores remains an important goal. With this in mind, we have developed the synthesis of pyrazinacene chromophores whose excitation and emission spectra fall within the tissue transparency window and whose quantum yields of fluorescence make them of significant interest for various applications.

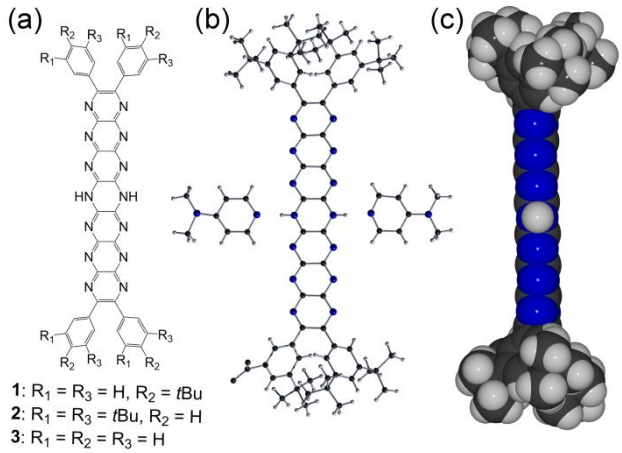

Figure 1. (a) Chemical structures of the 7,16-dihydro-1,4,5,6,7,8,9,10,13,14,15,16,17,18-tetradecaazaheptacene derivatives **1** and **2**. Structure **3** was used for computational purposes. (b) X-ray crystal structure of **2**. Two 4-DMAP molecules are hydrogen bonded (N_{14}Hp...N_{DMAP} 2.69 Å) at central dihydropyrazine. (c) Space-filling model viewed perpendicular to pyrazinacene plane.

Here we report the synthesis, amphiprotism and NIR emissive properties of an extended pyrazinacene chromophore containing 7 linearly-fused pyrazine units, i.e., tetradecaazaheptacene. Synthesis of **1** and **2** (Figure 1) was

achieved by the respective condensation of the appropriately substituted pyrazinopyrazine-2,3-dicarbonitrile with pyrazine-2,3,5,6-tetraamine.[10] This reaction ought to supply the tetrahydro derivatives but the corresponding dihydro derivatives were isolated. This is due either to autoxidation of the initial product or reaction of already oxidized derivatives of pyrazinetetramine. Final products were isolated in poor to moderate yields of around 16 % due to the requirement for a double condensation and the low stability of the pyrazinetetramine precursor. Solubilizing substituents were attached at the terminal carbon atoms of the tetradecaazaheptacene core rather than at nitrogen atoms in order to allow study of protic processes (protonation/deprotonation). The X-ray crystal structure of **2** is shown in Figure 1b, c (see also Figures S1, S2). Crystals were grown from solutions containing 4-dimethylaminopyridine (4-DMAP) to disclose the positions of the protons on the tetradecaazaheptacene ($N_{14}Hp$) backbone (triethylamine (TEA) was also used for this purpose but gave only poor quality crystals although the connectivity of its $N_{14}Hp$ backbone could still be established - Figures S3, S4). Two DMAP molecules per $N_{14}Hp$ are clearly contained hydrogen bonded ($N_{14}Hp$…N_{DMAP} 2.69 Å suggests a moderately strong interaction) with the structure of the central unit confirming that the dihydropyrazine compound was isolated. **2**.$DMAP_2$ units are arranged in the crystal with dimethylamino groups separating the $N_{14}Hp$ units (short contacts suggesting CH…π and CH…N interactions). Planes of the $N_{14}Hp$ chromophores are separated by ~6.8 Å.

Basic photophysical properties of the compounds are summarized in Figures 2, 3 and Table 1. Tertiary-butyl substituted compounds exhibit an absorption λ_{max} around 674 nm in methanol with a typical acene vibronic structure. The absorption edge at around 723 nm equates to an optical gap of 1.71 eV, very close to that of CH-only hexacene (1.79 eV).[11] Fluorescence emission occurs with a small Stokes shift of 20 nm. The excitation spectra of the neutral compounds in THF (Figure S5) are essentially identical with their absorption spectra, suggesting predominance of a single non-aggregated species, despite the possibility of numerous other tautomeric forms.[12] In low polarity solvents such as dichloromethane or toluene, acene-type spectra of **1** are replaced by a broad, hypsochromically shifted absorption at 604 nm, most likely as a result of aggregation (see Figure S6, S7). Aggregation of **1** under these conditions is also evident from ^{1}H NMR spectra, which reveal significant broadening of aromatic proton resonances (Figure S8). This can be eliminated by the addition of polar solvents such as DMSO, or by protonation or deprotonation. For **2**, aggregation is substantially eliminated at concentrations suitable for UV-vis (see Figure S7) and a typical acene vibronic structure was observed as shown in Figure 2 (a shoulder in the UV-vis spectrum at 705 nm suggests the presence of small quantities of either monoanion or aggregates). Protonation of **1** with TFA is complete after addition of one equivalent of acid (Figure 3, Figures S9, S10) and results in a hypsochromically shifted absorption spectrum with a λ_{max} of 575 nm for **2** in acetonitrile, and vibronic structure typical of acenes. Deprotonation (Figure 3) occurs using relatively weak bases such as DMAP or TEA leading to a bathochromically shifted absorption spectrum with a λ_{max} of 714 nm in methanol (for **1**) still with a characteristic acene vibronic structure. Deprotonation was confirmed by titration which fit well to a 1:1 process irrespective of the type of base used (for example, see Figure 3b, Figures S11, S12), and also by back titration with TFA where one equivalent was required to revert back to the spectrum of the neutral species. Surprisingly, deprotonation also occurs by dissolution in proton accepting solvents such as DMSO as evidenced by the significantly red-shifted absorption λ_{max} of 737 nm for **1**, which was not further deprotonated by addition of DMAP or TEA, and a two-step protonation upon reverse titration with methanesulfonic acid (see Figure S13, S14). The excitation spectrum of the deprotonated species is also identical to its absorption spectrum, again indicating a single predominant fluorescent species (Figure S15). Protonated species behave similarly (Figure S16). pK_a values of **2** were estimated by UV-vis titration of **2** with methanesulfonic acid (MSA) or DMAP in acetonitrile (MeCN) at 25 °C. This approach yields two pK_a(MeCN) values for **2**: pK_{a1}(MeCN) = 12.4 and pK_{a2}(MeCN) = 20.8. These values (relative to pK_s(MeCN)) indicate, respectively, that monoprotonation and monodeprotonation are relatively easy processes for **2** in MeCN.

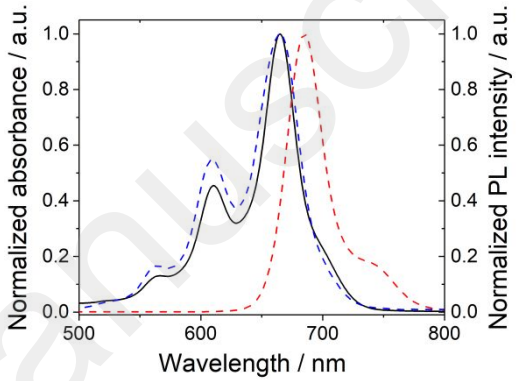

Figure 2. Electronic absorption spectroscopy of **2**. UV-vis (solid black line), fluorescence emission (dashed red line) and excitation (λ_{EX} = 690 nm, dashed blue line) spectra in THF.

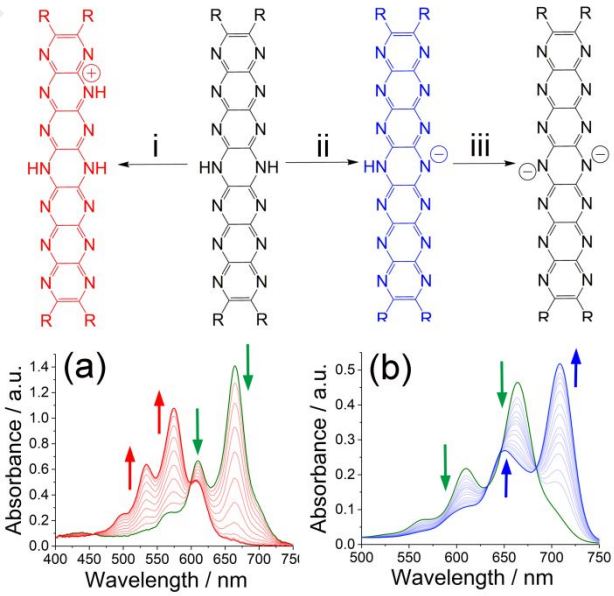

Figure 3. Prototropic reactions of $N_{14}Hp$ with (i) trifluoroacetic acid (proton at computationally most stable position), (ii) 4-dimethylaminopyridine (4-DMAP), (iii) lithium bis(trisilyl)amide. Color of the structures correspond to the endpoints of titrations shown in (a, b). (a) UV-vis titration with TFA. (b) UV-vis titration with 4-DMAP in acetonitrile. Arrows indicate variations in absorbance during titration.

The gas-phase deprotonation enthalpy (DPE) was calculated using the semi-empirical AM1 method as implemented in the Spartan '14 program (see Supporting Information). Compound **1** has a calculated DPE of 311.3 kcal/mol similar to that of the highly nitrogenated, electron deficient tetrapyrazinoporphyrazine (316.1 kcal/mol), which readily deprotonates upon dissolution in DMSO.[13] To effect further deprotonation, the use of a large excess of hydroxide or more strongly basic lithium bis(trimethylsilyl)amide is necessary and results in the formation of the doubly deprotonated species with a λ_{max} = 741 nm in THF (compound **1**, see Figure S17). The difficult second deprotonation of **1** is consistent with its high calculated DPE of 743.8 kcal/mol. Overall, the optical gap of these materials can be effectively tuned from around 2.2 eV to 1.6 eV by protonation, neutralization or deprotonation.

Table 1. Photophysical Properties of 1 and 2 including Photoluminescence Quantum Yields, Φ_{PL}

		Neutral				Deprotonated (TEA)				Protonated (TFA)			
	Solvent[a]	λ_{max}	ε (× 10^{-5}) (M^{-1} cm^{-1})	Em. λ_{max}	Φ_{PL}	λ_{max}	ε (× 10^{-5}) (M^{-1} cm^{-1})	Em. λ_{max}	Φ_{PL}	λ_{max}	ε (× 10^{-5}) (M^{-1} cm^{-1})	Em. λ_{max}	Φ_{PL}
1	THF	653	1.14	680	49.4	697	1.41	714	30.4	587	0.99	603	39.9
	MeCN	668	1.04	688	n.d.	701	1.19	727	n.d.	580	0.92	601	n.d.
	MeOH	676	1.23	697	n.d.	714	1.83	737	n.d.	603	1.13	629	n.d.
2	THF	644	1.18	689	42.1	692	1.19	712	57.7	582	0.95	597	42.4
	MeCN	665	1.22	686	60.9	705	1.65	730	51.2	575	0.95	595	48.3
	MeOH	671	1.21	693	40.8	710	1.76	732	31.6	598	0.98	656	30.3

[a]THF: tetrahydrofuran; MeCN: acetonitrile; MeOH: methanol.

Photoluminescence quantum yields (PLQYs) of the compounds (Table 1) were measured in different solvents. Generally, PLQYs are higher prior to treatment with acid or base. Compound **2** exhibits a large PLQY of 61% in acetonitrile with fluorescence λ_{max} = 686 nm. Deprotonation (in acetonitrile) results in a reduced PLQY (51%), and a bathochromic shift of emission further into the NIR region with a λ_{max} = 730 nm. Although deprotonation results in a slight decrease in PLQY, the extinction co-efficient at λ_{max} is increased somewhat from 1.22×10^5 to 1.65×10^5 $M^{-1}cm^{-1}$. The protonated species is less fluorescent than either the neutral species or the deprotonated species with a PLQY of 48 %.

Density functional theory (DFT) calculations were performed at the B3LYP/def2-TZVP level of theory on the N_{14}Hp compound **3** (Figure 1) where t-butyls of **1**,**2** were replaced with hydrogen atoms (Figure S18), in order to investigate quantitatively their structural and photophysical properties. The computed optimized ground state molecular structure of **3** matches well the crystal structure of **2** (see Figure S19), including the planarity at 7,16-dihydropyrazine group, dissymmetry in the C-N bond lengths of the backbone, and the orientation of phenyl groups. HOMO and LUMO structures of **3**, which are energetically isolated from the other occupied and vacant MOs, are largely delocalized over the molecule having respectively π- and π*-type characteristics (Figure 4), and present a HOMO–LUMO gap of 2.5 eV. This gap is strongly attenuated for single and double deprotonations (2.06 eV for the anion [**3** – H]$^-$ and 1.75 eV for the dianion [**3** – 2H]$^{2-}$, (Figure S18, Figures S20, S21). Single protonation yields several possible tautomers (Figure S18, S22) and a HOMO–LUMO gap of 1.57 eV was obtained for the computationally most stable tautomer cation [**3**H]$^+$ with comparable HOMO–LUMO gaps computed for other tautomers. Absorption spectra of the neutral and deprotonated models in the gas phase were computed using time-dependent density functional theory (TD-DFT) (see Supporting Information). Despite being hypsochromically shifted compared to the observed spectra (ca. 80-100 nm (ca. 0.35 eV)), they confirm the experimentally observed trend upon deprotonation. λ_{max} at 550 nm (2.25 eV), for neutral **3**, 618 nm (2.08 eV) for anion [**3** – H]$^-$ and 664 nm (1.87 eV) for the dianion [**3** – 2H]$^{2-}$are predicted with intense absorption bands almost exclusively involving HOMO–LUMO electronic transitions (Table S3). The small Stokes shift of ca. 20-30 nm observed experimentally (Figure 2a) is reproduced in the computed emission bands with λ_{max} (em) of 585 nm (2.12 eV), for **3**, 654 nm (1.90 eV) for [**3** – H]$^-$ and 695 nm (1.78 eV) for [**3** – 2H]$^{2-}$ (Table S3). DFT modeling of the protonated species [**3**H]$^+$ also predicts a decrease in the HOMO-LUMO gap and a bathochromic shift in absorption relative to the neutral species with a strong absorption band at 849 nm (1.46 eV) at the lowest energies (Table S3). These findings are not consistent with experiments, which suggest an increase in HOMO-LUMO gap. This inconsistency could be due to counterion effects, tautomerism or aggregation. Nucleus-Independent Chemical Shifts ($NICS_{iso}(0)$,[14] Figure S23, S24) reveal a distribution of aromaticity on the N_{14}Hp core in **3**.[15,16]

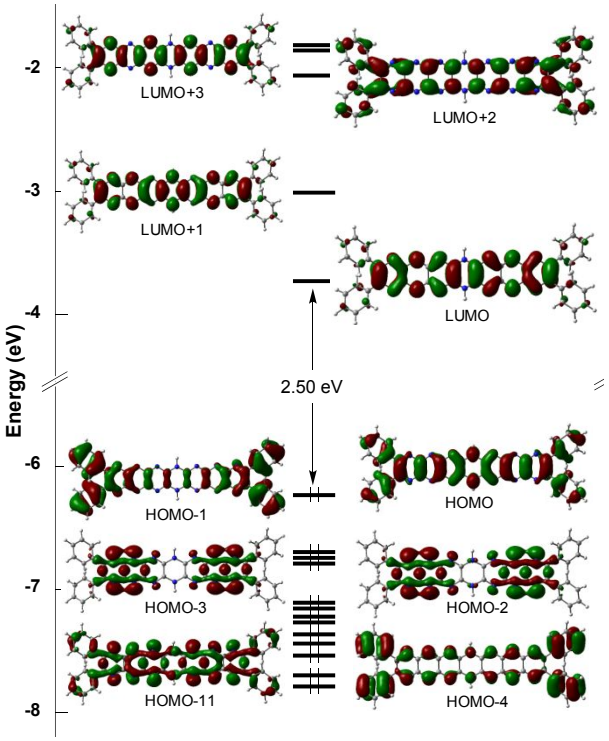

Figure 4. Calculated HOMO-LUMO molecular orbital structures of the model chromophore **3**. Contour values are ±0.03 $(e/bohr^3)^{1/2}$.

Although **2** can be obtained unaggregated in solution, the state and stability of **2** in films and solution was investigated. Compound **2** is stable indefinitely (years) under ambient dark storage conditions. When deposited on quartz substrate, **2** exhibits UV-vis spectra similar to those in non-polar solvents (i.e., aggregated, Figure S6, S25). Exposure of this film to acidic (TFA) or basic (TEA) vapor results in shifts of the UV-vis absorption maximum similar to those observed in solution suggesting formation respectively of monocation or monoanion in the aggregate films (Figure S26). Films of **2** exposed to direct sunlight were stable for several days with apparent gradual conversion to monocation (Figure S27(a)). Exposure to high intensity light from a Hg-Xe lamp leads to similar changes (Figure S27(c)) while, in CH_2Cl_2 solution, **2** undergoes rapid protonation followed decomposition (Figure S27(d)).

In summary, we report the synthesis of tetradecaazapyrazinacenes as an unprecedented class of long wavelength emissive chromophore with amphiprotic properties. The present work demonstrates that higher pyrazinacenes such as **1** and **2** are highly effective chromophores for NIR emission applications having excellent quantum yields of emission at 700 nm. The polar N_{14}Hp core with dihydropyrazine is stable even when deprotonated (does not autoxidize) and can be synthetically modified. These compounds are essentially monovalently amphiprotic undergoing single protonation/deprotonation (although double deprotonation is also possible). We are currently preparing other derivatives of the N_{14}Hp core for use as bio-imaging agents with the expectation that the oligopyrazine unit will lead to unique opportunities for selective imaging.

ASSOCIATED CONTENT

Supporting Information

The Supporting Information is available free of charge on the ACS Publications website at DOI: .
Details of synthesis, Cifs for **2**.$(DMAP)_2$ and the triethylamine solvate. Additional spectroscopic data. Computational methods. Plots of the computed compounds, selected DFT-optimized bond distances for **3**, DFT molecular orbital diagrams, NICS and TD-DFT data for $[\mathbf{3} - H]^-$, $[\mathbf{3} - 2H]^{2-}$, and $[\mathbf{3}H]^+$.

AUTHOR INFORMATION

Corresponding Authors

*richards.gary.james@ocha.ac.jp

*jonathan.hill@nims.go.jp

ORCID

Gary J. Richards: 0000-0002-5262-2587
Shinji Yamada: 0000-0002-5945-5996
Whitney A. Webre: 0000-0002-4777-2855
Paul A. Karr: 0000-0003-3560-2178
Jan Labuta: 0000-0002-8329-0634
Katsuhiko Ariga: 0000-0002-2445-2955
Francis D'Souza: 0000-0003-3815-8949
Jean-François Halet: 0000-0002-2315-4200
Jonathan P. Hill: 0000-0002-4229-5842

Notes

The authors declare no competing financial interests.

ACKNOWLEDGMENT

This work was partly supported by World Premier International Research Center Initiative (WPI Initiative), MEXT, Japan, JSPS KAKENHI Grant No. JP15K13684 (Linear acene proton conductors for molecular electronics), JSPS KAKENHI Grant No. JP16H06518 (Coordination asymmetry), and CREST JST, Japan (Grant No. JPMJCR1665). A.C., S.K., and J.-F.H. are grateful to GENCI (Grand Equipment National de Calcul Intensif) for HPC resources (Grant A0050807367). These studies were also facilitated within the scope of the France Japan International Collaboration Framework through the Laboratory for Innovative Key Materials and Structures (UMI 3629 LINK), financially supported by Saint-Gobain, Centre National de la Recherche Scientifique (CNRS), Université de Rennes 1 (UR1), and National Institute for Materials Science (NIMS). This work was financially supported by the National Science Foundation (Grant No. 1401188 to FD).

REFERENCES

(1) Richards, G. J.; Hill, J. P.; Subbaiyan, N. K.; D'Souza, F.; Karr, P. A.; Elsegood, M. R. J.; Teat, S. J.; Mori, T.; Ariga, K. Pyrazinacenes: aza analogues of acenes. *J. Org. Chem.,* **2009,** *74*, 8914–8923.

2. Richards, G. J.; Hill, J. P.; Mori, T.; Ariga. K. Putting the 'N' in acene: pyrazinacenes and their structural relations. *Org. Biomol. Chem.* **2011**, *9*, 5005–5017

(3) Švec, P.; Webre, W.; Richards, G. J.; Labuta, J.; Wakayama, Y.; Miklík, D.; Karr, P. A.; Mori, T.; Ariga, K.; D'Souza, F.; Hill, J. P. Phenanthroline-fused pyrazinacenes: One-pot synthesis, tautomerization and a $Ru^{II}(2,2'\text{-bpy})_2$ derivative. *Eur. J. Inorg. Chem.*, **2018**, *22*, 2541–2548.

(4) Escobedo, J. O.; Rusin, O.; Lim, S.; Strongin, R. M. NIR dyes for bioimaging applications. *Curr. Opin. Chem. Biol.* **2010**, *14*, 64–70.

(5) Barbieri, A.; Bandini, E.; Monti, F.; Praveen, V. K.; Armaroli, N. The rise of near infrared emitters: organic dyes, porphyrinoids and transition metal complexes. *Top. Curr. Chem.*, **2016**, *374*, 1–39.

(6) Baggaley, E.; Weinstein, J. A.; Williams, J. A. G. Lighting the way to see inside the lice cell with luminescent transition metal complexes. *Coord. Chem. Rev.* **2012**, *256*, 1762–1785.

(7) Porcu, E. P.; Salis, A.; Gavini, E.; Rassu, G.; Maestri, M.; Giunchedi, P. Indocyanine green delivery systems for tumour detection and treatments. *Biotechnol. Adv.*, **2016**, *34*, 768–789.

(8) Lu, H.; Mack, J.; Yang, Y.; Shen, Z. Structural modification strategies for the rational design of red/NIR region BODIPYs. *Chem. Soc. Rev.* **2014**, *43*, 4778–4823.

(9) Ogata, F.; Nagaya, T.; Maruoka, Y.; Akhigbe, J.; Meares, A.; Lucero, M. Y.; Satraitis, A.; Fujimura, D.; Okada, R.; Inagaki, F.; Choyke, P. L.; Ptaszek, M.; Kobayashi, H. Activatable near-infrared fluorescence imaging using PEGylated bacteriochlorin-based chlorin and BODIPY-dyads as probes for detecting cancer. *Bioconjugate Chem*. **2019**, *30*, 169–183.

(10) Donald D. S. Tetraaminopyrazine, 2,3,5-triamino-6-nitropyrazine and 2,6-diamino-3,5-dinitropyrazine. **1974**. US 3808209A (accepted patent).

(11) Mondal, R.; Shah, B. K.; Neckers, D. C. Photogeneration of heptacene in a polymer matrix. *J. Am. Chem. Soc.*, **2006**, *128*, 9612-9613.

(12) R. Scipioni, R.; Boero, M.; Richards, G. J.; Hill, J. P.; Ohno, T.; Mori, T.; Ariga, K. Tautomerism in reduced pyrazinacenes. *J. Chem. Theory Comput.,* **2010**, *6*, 2517-525.

(13) Stuzhin, P. A.; Malyasova, A. S.; Sheinin, V. B.; Kokareva, E.; Tarakanov, P. A.; Koifman, O. I. Acid-base properties of tetrapyrazinoporphyrazines. 1. Deprotonation of octaethyltetrapyrazinoporphyrazine in CH_2Cl_2, THF, DMSO and pyridine. The crucial role of water. *Dyes Pigm.*, **2017**, *139*, 509-516.

(14) Chen, Z.; Wannere, C. S.; Corminboeuf, C.; Puchta, R.; Schleyer, P. v. R. Nucleus-independent chemical shifts (NICS) as an aromaticity criterion. *Chem. Rev.* **2005**, *105*, 3842–3888.

(15) Miao, S.; Brombosz, S. M.; Schleyer, P. v. R.; Wu, J. I.; Barlow, S.; Marder, S. R.; Hardcastle, K. I.; Bunz, U. H. F. Are N,N-dihydrodiazatetracene derivatives antiaromatic? *J. Am. Chem. Soc.*, **2008**, *130*, 7339-7344.

(16) Wu, J. I.; Wannere, C. S.; Mo, Y.; Schleyer, P. v. R; Bunz, U. H. F. 4n π Electrons but stable: N,N-Dihydrodiazapentacenes. *J. Org. Chem.*, **2009**, 74, 4343-4349.